Improvements in classification of left and right foot motor intention using modulated steady-state somatosensory evoked potential induced by electrical stimulation and motor imagery

Yan Bian
Tianjin University of Technology and Education
Li Zhao
Tianjin University of Technology and Education
Jiaying Li
Tianjin University of Technology and Education
Tong Guo
Tianjin University
Xing Fu
Tianjin University
Hongzhi Qi (qhz@tju.edu.cn)
Tianjin University

Research Article

Keywords: brain–computer interface, motor imagery, foot motor intention recognition, steady-state somatosensory evoked potentials, task-related component analysis

Posted Date: April 18th, 2022

DOI: https://doi.org/10.21203/rs.3.rs-1545696/v1

Abstract

Background

In recent years, motor imagery-based brain-computer interface (MI-BCI) has been applied to motor rehabilitation in patients with motor dysfunction. However, traditional MI-BCI is rarely used for foot motor intention recognition because the motor cortex regions of both feet are anatomically close to each other, and traditional event-related desynchronization (ERD) patterns for MI-BCI have insufficient spatial discrimination.

Methods

This study introduced steady-state somatosensory evoked potentials (SSSEPs) by synchronous bilateral feet electrical stimulation at different frequencies, which were used as carrier signals modulated by unilateral foot motor intention. Fifteen subjects participated in MI and MI-SSSEP tasks. A Riemannian geometry classifier with a task-related component analysis (TRCA) spatial filter was proposed to demodulate the variation in SSSEP features and discriminate the left and right foot motor intentions.

Results

The feature outcomes indicated that the amplitude and phase synchronization of the SSSEPs could be well modulated by unilateral foot MI tasks under the MI-SSSEP paradigm. The classification results revealed that the modulated SSSEP features played an important role in the recognition of left-right foot discrimination. Moreover, the proposed TRCA-based method outperformed the other three methods and improved the foot average classification accuracy to 81.07 ± 13.29%, with the highest accuracy attained at 97.00%. Compared with the traditional MI paradigm, the foot motor intention recognition accuracy of the MI-SSSEP paradigm was significantly improved, from nearly 60% to more than 80%.

Conclusions

This work provides a practical method for left-right foot motor intention recognition and expands the application of MI-BCI in the field of lower-extremity motor function rehabilitation.

1 Background

A brain–computer interface (BCI) can replace, repair, enhance, supplement, or improve the normal output of the central nervous system and change its interaction with the internal/external environment[1]. In recent years, BCIs have been applied to the plasticity rehabilitation of limb motor ability in patients with amyotrophic lateral sclerosis, spinal cord injury, stroke, or other diagnoses, as they can promote the recovery of cerebral function or behavior by manipulating neurophysiological activities and represent a

potential rehabilitation method[2–3]. For example, in a lower-limb gait control system, BCIs can be exploited to effectively manipulate rehabilitation devices, such as foot nerve prostheses or gait orthoses[4], even for chronic stroke patients[5]. For motor recovery, whether the patient's motor intention can be correctly decoded is crucial to promote BCI performance.

Motor imagery (MI) refers to an inner cerebral process of motor behavior but without any actual body movement; therefore, MI-BCI is often used to detect patients' motor intentions and has been widely used in limb motor rehabilitation. In MI-BCI, an increase or decrease in electroencephalogram (EEG) energy occurs in alpha or beta frequency bands, mainly over the primary sensorimotor area during task periods, namely, event-related synchronization (ERS) and event-related desynchronization (ERD)[6–7], which are vital features to identify target MI and recognize corresponding motor intentions. However, in classical MI-BCI, the types of imagery paradigms are very limited[8–9], especially for lower-limb MI, where both feet are usually treated as one imagery paradigm without unilateral discrimination. The main reason is that in primary sensorimotor cortices, the foot area locates near the interhemispheric fissure[10–11], and thus, the left and right foot areas from the two cerebral hemispheres are anatomically close to each other. Due to low spatial resolution of EEG recordings, the left and right foot MI produce nearly identical EEG patterns[11–12], making the classification of left and right foot motor intention difficult. Therefore, few reports have focused on lower-limb motor intention discrimination. According to the available documents, the possible EEG features for foot unilateral classification are primarily mu-ERD, beta-ERD, and beta-ERS in traditional MI-BCI. However, these previous results seem controversial; one work reports an ERD/ERS left-right difference for all three features during a foot MI task[12]. In contrast, another similar study believed that mu-ERD and beta-ERD were not prominently lateralized for foot motor intention discrimination[11], and unlike the above two literatures, another study demonstrated both mu-ERD and beta-ERS exhibited no significant difference between left and right foot MI[13]. These conclusions indicate that ERD/ERS left-right foot discrimination may be unreliable and insufficient, which may be associated with MI paradigm, reference method, subject population, and so on. Moreover, the classification results for ERD/ERS left-right foot discrimination remain unsatisfactory, that is, the average accuracies of most studies are approximately 70%, which is unsuitable for practical applications. For example, for left-right foot discrimination, Hashimoto et al. reported an average classification accuracy of 69.3%[11], and Tariq et al. reported an average accuracy of 70.28%[14]. Recently, some studies have attempted to develop classification algorithms, such as common spatial patterns and their extensions, support vector machine (SVM)-based algorithms, and the k-nearest neighbor (KNN) classifier[10, 12, 14], to aid in enhancing left-right foot discrimination, but the small improvements could not facilitate the discrimination to a practical level. Therefore, further investigations are still essential to develop reliable features and methods for higher foot classification accuracy.

To find a reliable and discriminable feature that can lead to high classification accuracy for left-right foot discrimination, this paper introduces a different feature unlike the common ones mentioned in previous studies for foot motor intention recognition, namely, modulated steady-state somatosensory evoked potential (SSSEP), which is induced by electrical stimulation and MI tasks. SSSEP, as a type of steady-

state somatosensory characteristic potential, has been introduced into hybrid BCIs in recent years[15]. As it has been proven that the combination of SSSEP features and MI tasks can enhance the spatial resolution of MI recognition and improve the recognition accuracy of upper-limb classification performance[9, 16, 17], it is natural to assume the good performance of introducing SSSEP into MI-BCI for foot motor intention recognition. The electrical stimulation could produce a stable SSSEP of the same stimulation frequency and activate the cerebral sensory cortex. As it only relies on the human sensory system, somatosensory stimulation maintains the advantages of a traditional MI-BCI, as compared with visual or auditory stimulation. Furthermore, SSSEP could be modulated by left or right foot motor intention; the execution of a unilateral foot MI task would suppress the amplitude and phase synchronization of the SSSEP induced on the same site; consequently, the left and right foot motor intentions can be loaded on the modulated SSSEP. Therefore, the discrimination problem of spontaneous EEG signals with a low signal-to-noise ratio can be transformed into the demodulation of a reliable SSSEP feature with a high signal-to-noise ratio. Figure 1 shows a schematic diagram of MI-modulated SSSEPs.

In addition to introducing a new feature for left-right foot discrimination, a suitable modulation method is also proposed according to the lock-in time and phase properties of the SSSEP, namely, a Riemannian geometry classifier with a task-related component analysis (TRCA) spatial filter, which is sensitive to SSSEP variations. In addition, we also compare the proposed methods with other typical feature-extraction and classification algorithms, such as a filter bank common spatial pattern (FBCSP) algorithm and a SVM classifier, which is popular for MI-BCI, to analyze the classification performance of different paradigms, features, and methods.

2 Methods

2.1 Participants

Fifteen healthy subjects (seven male and eight female), with an average age of 23.7 ± 1.9 years, were recruited in this experiment. They were all college students with right-handedness, normal or corrected normal vision and sensation, and no history of trauma or neurological-related diseases. Before the formal experiment, each subject was trained for three days (half an hour each day) to familiarize themselves with electrical stimulation, MI tasks, and specific experimental processes as quickly as possible. During the training process, it is necessary to determine the left and right foot electrical stimulus amplitudes, as well as the stimulation position for each subject. On the day of the formal experiment, the subjects were in a good mental state without fatigue or physical discomfort. Before the experiment, all subjects were informed of the purpose and process of the experiment and provided signed informed. This study was approved by the ethics committee of Tianjin University.

2.2 Electrical stimulation

Somatosensory potentials can be evoked by electrical stimulation or vibration stimulation. Since electrical stimulation easily induces a stable somatosensory potential and has a relatively large amplitude, electrical stimulation was used to induce SSSEP in our experiment. In our study, two-channel current pulses with a pulse width of 0.2 ms were used to induce the SSSEP. Two-channel electrodes were placed at the posterior tibial nerve of the medial malleolus of both the left and right foot. The stimulation position was approximately 2–3 cm behind the medial malleolus of the feet. A saddle electrode (3.5 × 2.3 cm) was used to induce the SSSEP. Before the beginning of the formal experiment, the exact stimulation position and current stimulation intensity of each subject was adjusted to achieve the effect of initial toe contraction without any pain. The lower-limb electrical stimulation intensity of different subjects is generally between 10 and 25 mA, and there are individual differences in the optimal stimulation frequency among different subject [4]. To determine the general optimal stimulation frequency and avoid overlapping with the frequency bands of MI (i.e., alpha and beta bands), the stimulation frequency of the left foot usually ranges from 26 to 30 Hz, and that of the right foot ranges from 31 to 35 Hz. The preliminary experimental results showed that all stimulation frequencies mentioned above could induce a stable SSSEP, but the amplitude of the SSSEP was the most obvious at the 28/33 Hz combination. Therefore, we selected 28 Hz as the left-foot stimulation frequency and 33 Hz as the right-foot stimulation frequency for all subjects. In addition, the two stimulation channels of the left and right foot were executed simultaneously.

Figure 2 shows the device, the stimulation positions of both feet, and the stimulation results of the SSSEP signal induced by electrical stimulation in channel Cz of a typical subject. The peak frequencies of somatosensory characteristics were consistent with the electrical stimulation frequencies used in our study, which indicated that the SSSEP in the primary sensorimotor area could be effectively induced by using the above electrical stimulation parameters.

2.3 Experiment description

The two paradigms in this study, MI and MI-SSSEP, are explained as follows:

a. *MI* is a classical motor imagery paradigm. Under this experimental condition, the subjects needed to imagine the unilateral kinesthetic MI task of the left foot or right foot hook action according to a text prompt of “left foot” or “right foot” on a screen. The imagery task lasted for 5 s.
b. *MI-SSSEP* is a hybrid experimental paradigm, and the subjects needed to carry out the same kinesthetic MI task as in the MI paradigm under the condition of electrical stimulation. The duration of the task was 5 s. One second before the task, electrical stimulation started to respond to the movement. When electrical stimulation was applied to the left and right foot, the prompts of “<<- Prepare” or “Prepare!>>” appeared on the screen, and the subjects needed to prepare for the MI-SSSEP task. One second later, the prompt of “left foot” or “right foot” was displayed with a red “+” indicating that the unilateral MI task should be done under somatosensory stimulation during this period.

The time course of a single trial experiment is shown in Fig. 3. At the beginning, the black text “Prepare, please!” appeared on the screen, which remained there for 2 s. Then, the prompt “Prepare!” was shown on the screen in the MI-SSSEP paradigms, after which electrical stimulation was applied to the left and right foot at 28 Hz and 33 Hz, respectively, until the end of the task. The electrical stimuli of both feet were applied simultaneously, which was indicated by a red “+” on the screen. One second later, the experimental tasks started, and the corresponding prompts were displayed on the screen. After 5 s, the green text “Please take a break!” appeared on the screen to remind the subjects to relax during this period. After a random rest of 2–3 seconds, the next experimental trial started. Data from 80 trials were collected under each paradigm, including 40 trials of the left foot and 40 trials of the right foot, which appeared in a random order. Each session of the experiment contained 40 trials, and after each session, there was a rest of 3–5 minutes to prevent fatigue and keep the subjects in a good experimental state. The experimental paradigms were performed in the Psychtoolbox of the MATLAB software (MathWorks Company, USA).

During the experimental process, the participants were asked to avoid subtle body movements and reduce the number of blinks during the task. A SynAmps2 electrophysiological amplifier (Compumedics Corporation, Australia) and a 64-channel electrode cap (using the international standard 10–20 system) were used for EEG signal acquisition. Reference and ground electrodes were set to the left and right mastoids, respectively. Scan 4.5 software was used for EEG signal acquisition, display, and storage. The data preprocessing included removing useless electrodes (M1, M2, CB1, and CB2) and performing a common average reference. Subsequently, the data were filtered using a 5–100 Hz bandpass filter to eliminate irrelevant frequency bands. Afterwards, blind source separation technology was used to remove artifacts, such as electrooculogram and electromyography. Finally, the data were downsampled to 200 Hz for subsequent analysis.

2.4 ERD and SSSEP feature analysis

Time-frequency analysis is a method that can analyze signal variations in time and frequency; therefore, it is especially suitable for exhibiting changes in ERD and SSSEP under different experimental paradigms. To further study the neural activities in the sensorimotor cortex under different paradigms, the event-related spectral perturbation (ERSP) was calculated based on a short-term Fourier transform. The disturbance of the event-related spectrum of the task periods relative to the baseline time period was calculated[7, 18]. Typically, if $F_k(f, t)$ is the spectral estimate of trial k at frequency f and time t for n trials, the ERSP can be calculated as follows:

$$\mathrm{ersp}(f, t) = \frac{1}{n}\sum_{k=1}^{n}(F_k(f, t)^2) \quad (1)$$

In this study, the Hanning window was used for the short-term Fourier transform, with a window length of 256 points (the number of windows is set to 200). For the two experimental paradigms, the average ERSP

results of the Cz channel were calculated.

Brain topographic mapping is a method that reflects the spatial distribution of energy in a specific period and the frequency bands of EEG signals. It can directly represent the spatial distribution of energy values in different channels with different colors; therefore, it is also a classical analysis method in EEG analysis[19]. To further explore the modulated SSSEP features (27–29 Hz and 32–34 Hz) of the MI-SSSEP paradigm, a brain topographic map of the left/right foot task was constructed. A grand average brain topographic map of 60 leads was used to compare the differences in the spatial distribution characteristics of the SSSEP spectra.

This study further analyzed whether there were significant differences between the ERD or SSSEP features of left- and right-lateral tasks under the two paradigms. The spectrum values of each subject during the left-right foot tasks in the alpha, beta, or modulated SSSEP frequency bands were calculated on the Cz channel, and the Wilcoxon signed-rank test was used to analyze the modulation effect in the spectrum value using unilateral foot tasks to explore the potential reasons why the SSSEP features of the MI-SSSEP paradigm can be used for lower-limb task classification.

As a modulation signal influenced by MI, the phase synchronization of the SSSEP may also change during the MI task periods. Here, we employed interstimulus phase coherence (ISPC) to measure phase synchronization variations under somatosensory stimulation[17]. Assuming that f is the SSSEP frequency, the original EEG $S(t)$ is first filtered to the $[f-0.5, f+0.5]$ SSSEP band, and then the filtered signal $S^f(t)$ is segmented by a sliding window, which moves $1/f$ seconds between two adjacent sliding windows. The segmented signals are defined as $S_k^f(t)$, where k denotes the k-th segment. If $\hat{S}_k^f(t)$ represents the Hilbert transform of $S_k^f(t)$, then the k-th segment analysis signal $X_k^f(t)$ is expressed as Formula (2):

$$X_k^f(t) = S_k^f(t) + j\hat{S}_k^f(t) \quad (2)$$

ISPC can be defined as follows:

$$ISPC^f(t) = \left| \frac{1}{N} \sum_{k=1}^{N} \frac{X_k^f(t + k\Delta t)}{\left| X_k^f(t + k\Delta t) \right|} \right| \quad (3)$$

where Δt denotes the time interval $1/f$ seconds. The ISPC is the result of averaging N stimuli, where N is the number of stimuli contained in one second. The ISPC values are between 0 and 1. A value of 0 indicates that there is absolutely no phase synchronization, and a value of 1 indicates perfect phase synchronization.

To further study the separability of foot motor intention in the SSSEP, we calculated the grand average separability r^2coefficient during the execution of the left/right foot imagery task under the MI-SSSEP paradigm. The calculation process is shown in Formula (4)[17]. The sample signal,x_{pm_1}, of the SSSEP band was composed of several trials in a 28- or 33-Hz frequency band during the left-foot imagery task on the m-th specific channel, where N_{pm_1} is the sample length. x_{pm_2} is a sample signal composed of multiple trials in the SSSEP frequency band during the right-foot imagery task on the m-th channel of the same subject, N_{pm_2} is the sample length, and is the total number of subjects.

$$r^2{}_m(x_{pm\_1}, x_{pm\_2}) = \frac{1}{P}\sum_{p=1}^{15}\left[\frac{\sqrt{N_{pm\_1} \times N_{pm\_2}}}{N_{pm\_1} + N_{pm\_2}} \frac{mean(x_{pm\_1}) - mean(x_{pm\_2})}{std(x_{pm\_1} \cup x_{pm\_2})}\right]^2$$

4

2.5 Classification

2.5.1 Riemannian geometry classifier with TRCA spatial filter

1) TRCA spatial filter

The TRCA algorithm could exhibit maximal similarity among task blocks and extract task-related components by properly weighing the observed signals[20]. Assuming task-related signal $s(t) \in R$ and task-unrelated signal $n(t) \in R$, the observed multichannel signals $x(t) \in R^{N_c}$ are composed of the following (5):

$$x_j(t) = a_{1,j}s(t) + a_{2,j}n(t), j = 1, 2, ..., N_c$$

5

where j denotes the channel index, N_c is the number of channels, and $a_{1,j}$ and $a_{2,j}$ are the mixing coefficients of the j-th channel. Then, the task-related components, $s(t)$, can be recovered from a linear sum of the observed signal, $x(t)$. To ensure that the task-related components exhibit maximal temporal similarity among task trials, inter-trial covariance maximization should be converted. If $x^{(h)}(t)$ is the h-th trial of the observed signal, and $y^{(h)}(t)$ $(t = 1, 2, ...N_t)$ represents the estimated task-related component, then the covariance of all possible combinations of trials is summed as Formula (6):

$$\sum_{h_1, h_2=1, h_1 \neq h_2}^{N_t} C_{h_1h_2} = \sum_{h_1, h_2=1, h_1 \neq h_2}^{N_t} \sum_{j_1, j_2=1}^{N_c} w_{j_1} w_{j_2} Cov(x_{j_1}^{(h_1)}(t), x_{j_2}^{(h_2)}(t)) = w^T S w$$

6

where the symmetric matrix S is defined as follows:

$$S_{j_1 j_2} = \sum_{h_1, h_2 = 1, h_1 \neq h_2}^{N_t} Cov(x_{j_1}{}^{(h_1)}(t), x_{j_2}{}^{(h_2)}(t))$$

7

To bound the coefficients, the variance of $y(t)$ is restricted as follows:

$$\begin{aligned} \mathrm{var}(y(t)) &= \sum_{j_1, j_2 = 1}^{N_c} w_{j_1} w_{j_2} Cov(x_{j_1}(t), x_{j_2}(t)) \\ &= w^T Q w = 1 \end{aligned} \quad (8)$$

The restricted optimization can be solved using Formula (9):

$$\hat{w} = \underset{w}{\mathrm{argmax}} \frac{w^T S w}{w^T Q w}$$

9

The optimal coefficient vector is obtained as the eigenvector of the matrix $Q^{-1}S$. The eigenvalues of matrix $Q^{-1}S$, which can be arranged in descending order, imply task consistency among the experimental trials[21]. In our study, we used the TRCA method to design spatial filters during task interval (0–3 s, where 0 s represented the start of the MI task) to obtain the SSSEP task-related components. In addition, this method can reduce the feature dimensions for Riemannian geometry measurement classification.

2) Data partitioning, multi-trial reference, and feature extraction

Considering there can be no overlap between the training set and the test set for constructing the spatial filter and task classification, the MI-SSSEP task interval signals were first divided into a training set and a test set according to the 10×10-fold cross validation method. Subsequently, the training set was filtered by 27–29 and 32–34 Hz sub-bands, and then the filtered multiple training trial data X_{train}^{28}, X_{train}^{33} were used to build TRCA spatial filters. The first two eigenvectors were employed to obtain the averaged task-related component, y_{ref} which was used as a reference after averaging for multiple training trials. Afterwards, the training and test trials were filtered by TRCA filters separately, and the task-related components y_{train} and y_{test} were covaried with the reference components, whose results were used as feature vectors for the Riemannian geometry measurement.

3) Riemannian geometry measurement

The Riemannian distance can be used to classify left-right foot motor intentions by calculating the Riemannian distance for each class. Here, given two samples, x_i and x_j, the Riemannian distance between them can be computed, as shown in Formula (10)[22]:

$$\delta_R\left(\sum_i, \sum_j\right) = \left\|\log\left(\sum_i^{-1/2}\sum_j\sum_i^{-1/2}\right)\right\|_F$$
$$= \left[\sum_{c=1}^{C}\log^2\lambda_c\right]^{1/2}$$

10

where \sum {_{i}} represents the covariance matrix of {x}_{i}, \sum {_{j}}denotes the covariance matrix of {x}_{j}, {\lambda _c}(c=1, \ldots ,C) are the real eigenvalues of {\sum {_{i}} ^{ - 1/2}}\sum {_{j}{{\sum {_{i}} }^{ - 1/2}}}, and is the number of channels. The Riemannian geometric mean of M covariance matrices is defined by the matrix that minimizes the sum of the squared Riemannian distances, as shown in Formula (11):

\mathfrak{G}(\sum {_{{1, \ldots ,}}} \sum {_{M}})=\mathop {\arg \hbox{min} }\limits_{{\sum { \in P(C)} }} \sum\limits_{{i=1}}^{M} {{\delta _R}^{2}(\sum {,\sum {_{i}})} } } (11)

4) Classification

Given a training set and the corresponding labels, {r_i} \in \left\{ {1,2} \right\} (1: left-foot motor intention; 2: right-foot motor intention), the training of the classifier estimates the Riemannian geometric mean for each class as follows (12):

\sum\limits_{{}}^{ - } {_{K}=} \mathfrak{G}\left. {(\sum {_{i}} } \right|{r_i}=K) (12)

where K \in \left\{ {1,2} \right\} denotes the class label. The classification of a test trial can be obtained by computing the minimum Riemannian distance to each class, as shown in Formula (13):

\hat {r}=\mathop {\arg \hbox{min} }\limits_{K} {\delta _R}(\sum\limits_{{}}^{ - } {_{K},\sum) } (13)

where \hat {r} denotes the predictive class. To ensure the reliability of the classification results, a 10×10-fold cross validation was performed to identify the left or right foot motor intention. Figure 4 shows diagrams of the proposed method.

2.5.2 Baseline classification algorithm

An FBCSP based on multiple frequency spatial filtering is selected as the baseline classification algorithm under different experimental paradigms, as it is a popular method in BCI applications[14, 23]. The composition of the FBCSP algorithm includes the following steps: first, the original EEG data were filtered through the N bandpass filters to form multiple sub-band EEG data. For each sub-band dataset, a binary CSP algorithm was used to design a spatial filter based on the training set, and the calculation formula of the CSP features in a single trial was obtained as Formula (14):

{v_{i,b}}=w_{i}^{T}{x_{i,b}}

14

where {x}_{i,b} is the EEG data after bandpass filtering of the b-th trial and the i-th frequency band, {w}_{i} is the spatial filter matrix of the corresponding frequency band, T represents the matrix transpose

operation, and {v}_{i,b} represents the feature matrix of the b-th trial and the i-th frequency band for each class. The first mmaximum and minimum eigenvalues were selected to form a spatial filter; therefore, 2×m eigenvectors were obtained in each sub-band of every trial under two unilateral tasks. Subsequently, all the feature vectors in the n-th sub-bands were combined, and then the motor intention was decoded by the SVM classifier, which is also a classical method in BCI pattern recognition[24, 25].

According to the FBCSP algorithm process, the training-set data were filtered by different sub-bands, which mainly included alpha and beta bands, as well as the first- and second-harmonic bands of the SSSEP stimulation frequency. The specific frequency bands were occupied at 8–13, 13–26, 27–29, 32–34, 55–57, and 65–67 Hz. These six sub-bands were then selected to construct a spatial filter. After bandpass filtering of each sub-band in the training process, the FBCSP algorithm was used to build a spatial filter model, and the first two maximum and minimum eigenvalues were selected to form a spatial filter in our study. Afterwards, the spatial filter model was used in the bandpass filtered data of the test set to obtain the feature vectors of each sub-band. After combining the features of all sub-bands, an SVM classifier was used to obtain the classification accuracies. To ensure the reliability of the classification results, a 10×10-fold cross validation was performed, and only training data were involved in forming a spatial filter or SVM classifier model during the process. The results of decoding accuracy recognition among the two experimental paradigms were analyzed by the Wilcoxon signed-rank test to explore whether the accuracy of the MI-SSSEP paradigm was significantly higher than that of the MI paradigms. Moreover, the classification performances were evaluated using different features (i.e., ERD/SSSEP/hybrid features) for the MI-SSSEP, and the one-way repeated measurement ANOVA with Bonferroni post-hoc test was conducted with the classification results to explore whether the modulated SSSEP feature played a crucial role under the MI-SSSEP paradigm in improving the classification results. In addition, to explore the optimal classification methods for the modulated SSSEP features, comparisons of the proposed TRCA-based Riemannian classification method with another three methods, including the baseline method, were further investigated.

3 Results

3.1 ERD and SSSEP features

The characteristic variations in the grand average ERSP with time and frequency under the experimental paradigms are shown in Fig. 5(a). This figure shows that the energies of the alpha and beta bands decreased during the imagery task periods under the MI and MI-SSSEP paradigms, which indicated that ERD phenomena occurred in both paradigms. In addition, under the MI-SSSEP paradigm, SSSEP features occurred at 28 and 33 Hz after the beginning of electrical stimulation and lasted until the end of electrical stimulation, and the features induced on the Cz channel were extremely obvious. This phenomenon was consistent with the conclusion that the left and right foot cerebral mapping areas were located near the interhemispheric fissure. To further explore the spatial distribution characteristics of the modulated SSSEP features, we selected data from 0.5–4.5 s after the start of the imagery task and calculated the

brain topographic map distribution results of grand average SSSEP features at all 60 electrodes, as shown in Fig. 5(a). The spatial distribution results under the MI-SSSEP paradigm revealed that the areas of somatosensory characteristics at 28 and 33 Hz were mainly distributed near the midline of the central area. Moreover, when performing different unilateral MI tasks, the spatial distributions of SSSEP features at different stimulation frequencies under the MI-SSSEP paradigm also appeared to vary, indicating that the unilateral MI tasks could modulate the SSSEP signals well.

From the temporal-spatial-frequency analysis results of EEG under the different experimental paradigms, the MI-SSSEP paradigm exhibited an EEG pattern that included both ERD and SSSEP features. However, the features that play a key role in the improvement of BCI classification performance in left/right foot motor intention discrimination still needed to be clarified. To select separable features from the hybrid paradigm, we further analyzed the ERD and SSSEP features on the Cz channel for the two experimental tasks. Figure 5(b) shows the grand average alpha and beta ERD characteristics in the MI and MI-SSSEP paradigms when performing the left/right foot hooking MI task. The results of the Wilcoxon signed-rank test showed that there was no significant difference in ERD characteristics between the left and right foot tasks in either the MI or MI-SSSEP paradigm (MI paradigm alpha: $P = 0.5000 > 0.05$, beta: $P = 0.4102 > 0.05$; MI-SSSEP paradigm alpha: $P = 0.1250 > 0.05$, beta: $P = 0.4551 > 0.05$). Therefore, ERD features alone did not provide a sufficient separation effect on foot movement intention recognition. The Wilcoxon signed-rank test was also used to analyze the grand averaged SSSEP features on the Cz channel under the MI-SSSEP paradigm. The results showed that there were statistically significant differences between the average power spectrum values of the left and right foot MI tasks at the two sensory stimulation frequencies under the MI-SSSEP paradigm (SSSEP 28 Hz: $P = 0.0075 < 0.01$, SSSEP 33 Hz: $P = 0.0416 < 0.05$), as shown in Fig. 5(b). These results implied that the SSSEP could be well modulated by the MI tasks. Moreover, the SSSEP variations were well separable as motor intention carrier signals under the MI-SSSEP paradigm. Subsequently, we further computed the grand average {r}^{2} coefficient topographic map of 60 channels during the foot imagery tasks under the MI-SSSEP paradigm, as shown in Fig. 5(c). The results demonstrated that the separability features mainly distributed in the sensorimotor area of the central area, which agreed with the modulated SSSEP topographic maps. Therefore, it was inferred that the SSSEP features of the sensorimotor cortex could provide good separability for discriminating foot motor intention.

The MI tasks not only had a significant impact on SSSEP amplitudes, but also changed the phase synchronization in the MI-SSSEP, as shown in Fig. 6(a). The grand average ISPC curves on the Cz channel demonstrated that the phase synchronization could be improved rapidly after the beginning of electrical stimulation, and that ISPC values decreased approximately 0.5 s ahead of the end of somatosensory stimulation. Therefore, the electrical simulation caused fine phase synchronization at the same stimulation frequencies. In particular, the unilateral MI task obstructed the phase synchronization of the ipsilateral stimulation frequency; for example, when implementing the left foot MI task, the ISPC value of 28 Hz decreased dramatically from the start of the MI task because the left-foot stimulation frequency was 28 Hz, but while fulfilling the right-foot MI task, the phase synchronization of 28 Hz was not influenced during the MI task period, and vice versa.

To further study the ISPC feature discrepancy between two unilateral foot MI tasks, the {r}^{2} coefficient and corresponding topographical maps at different times were compared, as seen in Fig. 6(b). As shown in the lower panel of Fig. 6, the ISPC revealed a high discrepancy during the MI task period, and the topographical maps of the {r}^{2} coefficient spatial distributions showed that the ISPC discrepancies between left-right foot motor intentions mainly focused on the sensorimotor area near the central area, which was consistent with the previous results shown in Fig. 5(c). These findings verified that both the amplitude and phase synchronization of the modulated SSSEP under the MI-SSSEP paradigm were closely related to unilateral foot MI tasks and different motor intentions.

3.2 Classification performance

The modulated SSSEP features of the MI-SSSEP paradigm were significantly different between the left-right foot motor intentions, which provided a basis for the separability of the foot imagery task at the feature level. However, whether the EEG signals in the SSSEP bands exhibited elevated separability after TRCA spatial filtering was vital to determine the final classification performance. Therefore, the separability of the EEG signals before and after the TRCA w-28/w-33 spatial filters was further analyzed. The TRCA-based filtered results are shown in Fig. 7. The left panel in Fig. 7(a) shows the {r}^{2} time-frequency maps of data filtered by the w-28/w-33 TRCA spatial filter of a typical subject, which revealed that the filtered data still maintained good separability after the TRCA filtering, especially during the 0–3 s after the start of the MI task. The right panel in Fig. 7(b) displays the statistical comparisons of the grand average {r}^{2} coefficients before and after the TRCA filter. The two violin plots indicated that TRCA filtering by w-28 and w-33 could both significantly improve the SSSEP discrepancies ($P < 0.001$); thus, as a carrier signal modulated by unilateral MI tasks, such a substantial promotion was determined to improve foot motion intention recognition based on the TRCA spatial filter method.

Comparisons of recognition performance for different features and methods are exhibited in Fig. 8. Figure 8(a) revealed that there was a significant classification accuracy difference using the baseline method among different features for the MI-SSSEP paradigm (one-way repeated measurement ANOVA: $F(1.062,14.867) = 15.297$, $P = 0.001$). The accuracies of applying hybrid and SSSEP features both significantly outperformed only using ERD features, with P values of 0.001 and 0.014, respectively, while there was no significant classification difference between employing hybrid and SSSEP features ($P = 0.155$). These results may indicate that the modulated SSSEP features played an important role in discriminating foot MI tasks for the MI-SSSEP paradigm due to the good discrepancies. There was no obvious accuracy difference with different features for the MI paradigm (hybrid vs. ERD features). In addition, the Wilcoxon signed-rank test results indicated that the classification accuracy of the MI-SSSEP paradigm was significantly higher than that of the MI paradigm using hybrid features ($P = 0.0013$), with the average accuracy of 15 subjects able to be improved from 59.57–71.22%. However, the statistical results shows that there was no significant difference in classification performance between the MI-SSSEP and MI paradigms ($P = 0.4670 > 0.05$) when both applied ERD features.

To further explore the optimal classification method for the modulated SSSEP features, the classification outcomes are recalculated with four different methods, including the proposed TRCA-based Riemannian

geometry method (TRCARIE), TRCA-based SVM method (TRCASVM), FBCSP-based Riemannian geometry method (FBCSPRIE), and the baseline method of FBCSP-based SVM classifier (FBCSPSVM). Figure 8(b) shows the classification results of these methods using two basebands of SSSEP features under the MI-SSSEP paradigm. The best average accuracy of 15 subjects further reached 81.07% for the MI-SSSEP paradigm, with the maximum individual accuracy reaching 97.00%, as obtained by the proposed TRCARIE method. Moreover, the classification accuracy of the TRCARIE method significantly outperformed the other methods, namely, the TRCARIE versus baseline method, with the average accuracy increased by 16.41% ($P = 0.002$). These results showed that for the MI-SSSEP paradigm, the TRCA filter with the Riemann classifier could effectively recognize the left-right foot motor intention and was thus especially suitable for the identification of SSSEP carrier signals. Furthermore, a two-way repeated measurement ANOVA confirmed the main effects of the feature method on the accuracy were statistically significant ($F(1,14) = 13.185$, $P = 0.003 < 0.01$); the same was the case for the classification method ($F(1,14) = 20.718$, $P < 0.001$), and there was no significant interaction between them. These results may indicate that applying the TRCA or Riemannian geometry methods both could improve the recognition accuracy, and this may explain why the accuracy of the traditional baseline method (FBCSPSVM) was significantly lower than that of the other three methods under the MI-SSSEP paradigm. In addition, across individuals, 73.3% of subjects (11 out of 15) achieved an accuracy higher than 70% using TRCARIE methods, and 26.7% of subjects (4 out of 15) obtained an accuracy higher than 90%, which demonstrated that for the MI-SSSEP paradigm, using the proposed method could effectively distinguish foot MI tasks for most subjects and improve the BCI recognition performance to a practical level. Unlike the results of MI-SSSEP, the average accuracies of the MI paradigm indicated that there were no significant differences between the four methods, which may be caused by the poor separability of the two ERD bands.

4 Discussion

The recognition of left and right foot motor intention is an onerous problem because the motor cortex regions of both feet are anatomically close to each other. Hence, the conventional MI paradigm has difficulty solving left-right foot discrimination problems, which is mainly due to the lack of reliable and discriminable features. As shown in Fig. 8(a), the classification accuracy using only ERD features was less than 70%, which was consistent with previous studies[11]. Figure 8(a) also indicated that the classification accuracy using modulated SSSEP features significantly outperformed that using ERD features, obtaining a similar classification efficiency as using both features under the MI-SSSEP paradigm. These results implied that using SSSEP features was better than ERD features in 2-class foot motor intention recognition in our study. Figures 5 and 6 proved our hypothesis that SSSEP features could be modulated by the ipsilateral MI task, which influenced both the amplitude and phase synchronization, resulting in a new reliable feature for foot left-right discrimination. The modulation effect may be due to the execution of the MI task sharing some sensory neuronal clusters with the sensory resources used to generate SSSEP. Therefore, the amplitude and phase synchronization of SSSEP were suppressed during the ipsilateral MI process as a result of resources competition, while the

MI activity had little effect on the SSSEP produced at the contralateral site. Obviously, this top-down neural modulation process was related to the action–perception coupling and interaction of the neuronal populations underlying the primary sensorimotor area and will bring new ideas to the development of BCI paradigms. In addition, the SSSEP was a narrow-band signal related to the stimulation frequency; as a carrier signal under the MI-SSSEP paradigm, the unilateral information was compressed into a narrow band based on modulation and demodulation effects, enhancing the signal-to-noise ratio of the useful information, and this may explain why the separability of SSSEP features was better than that of ERD features in this study. More importantly, the highest average classification accuracy (15 subjects), obtained by using two bands of modulated SSSEP features, reached 81.07 ± 13.29% under the MI-SSSEP paradigm, an improvement of nearly 20% compared with the average accuracy only using ERD features, which indicated more notable and more likely improvements for foot unilateral classification. To our knowledge, this study is the first to introduce modulated SSSEP as a new feature to discriminate left-right foot motor intention and significantly improves the average classification accuracy to a practical level; thus, the current work provides a novel way of lower-extremity motor function rehabilitation.

Our study used two paradigms: the proposed MI-SSSEP paradigm and the traditional MI paradigm. The experimental results suggested that the introduction of modulated SSSEP features could significantly improve the classification performance of the MI-SSSEP paradigm compared with the traditional MI paradigm when performing the identical MI task. Furthermore, based on the individual classification of 15 subjects under the MI-SSSEP paradigm, 73.3% of subjects achieved more than 70% accuracy using the proposed method, and 26.7% of subjects achieved more than 90%. Due to the obvious individual differences and low accuracy in MI-BCI, the MI-SSSEP paradigm is expected to not only provide feasible foot motor intention discrimination but also supply a practical way to improve the recognition efficiency for most subjects. In our previous research, we tried to apply electrical stimulation to an upper-limb MI task, which was used to recognize the motor intention between the left and right hands or to distinguish the motor intention between the right hand and Ipsilateral arms. Compared with the single MI task, the classification accuracy was improved by more than 10%[9, 16]. The current work verified the effectiveness of using SSSEP features in lower-limb motor intention recognition, and it can be supposed that the SSSEP features generated during the MI task could help to enhance the spatial resolution of MI recognition and extend the numbers of limb imagery actions in MI-BCI, such as left/ right foot or right foot/right knee MI tasks. In addition, since the production of SSSEP depends on the human body's own sensory system, the coactivation mode of the sensory cortex and motor cortex is closer to the oscillation mode of traditional MI-BCI, as compared with other types of hybrid paradigms.

To obtain optimal results for foot motor intention recognition, the demodulation method is worthy of intensive study. Figure 8(b) displays the classification performance of the four methods used in this study, which demonstrate that the proposed Riemannian geometry with the TRCA spatial filter method was best for left-right foot discrimination under the MI-SSSEP paradigm. Although there is no report involving the TRCA method used for SSSEP feature extraction, several works reported that the TRCA method showed good performance in extracting task-related components, such as steady-state visual

evoked potential (SSVEP)[20, 21]. In terms of the time-locked characteristics of the SSSEP signal compared to that of SSVEP, it is natural to assume that the TRCA spatial filter has good performance in SSSEP feature extraction. As shown in Fig. 7(b), the SSSEP separability after TRCA spatial filtering was further significantly improved compared with that using pre-filtered signals, and the feature extraction methods had a significant effect on improving the classification accuracy (TRCA vs. FBCSP methods). Moreover, the statistical results demonstrated the Riemannian geometry classifier could also obtain higher classification performance for the MI-SSSEP paradigm than that of the SVM classifier. The Riemannian distance measurement can take the advantages of both temporal information and spatial information simultaneously, rather than using single information as traditional measurements; thus, this method could facilitate the classification of the modulated SSSEP, which is characterized in both time and frequency domains. Therefore, the proposed method was especially adapted for the MI-SSSEP paradigm as an ideal demodulation algorithm for the modulated SSSEP carrier signals. However, for the MI paradigm, the proposed method did not exhibit good performance. Possible explanations are that the separability of ERD features was not strong in our study, and the ERD features did not have as good of time-locked and phase-locked characteristics compared to SSSEP features; consequently, the TRCA method may be unsuitable for processing ERD features.

Considering the important applications of MI-BCI in the field of motor rehabilitation, the method proposed in this paper not only successfully elicited modulated SSSEP features but also significantly improved left-right foot classification accuracy by using the modulated features. Of course, the introduction of SSSEP into MI-BCI also brings some negative aspects, such as increasing system complexity and being unsuitable for somatosensory pathway impaired patients. However, considering there are many patients whose somatosensory system is intact, this study could provide a new feature, method, and experimental data support to control rehabilitation devices of lower-limb motor function for such a population.

5 Conclusions

In this study, based on somatosensory stimulation and MI-BCI, a new feature and method for foot unilateral motor intention recognition was proposed. SSSEP signals induced by electrical stimulation were used as carrier channels, and the unilateral foot motor intention could change the amplitude and phase synchronization of the ipsilateral SSSEP. The Riemannian geometry with a TRCA spatial filter method was introduced in this study to demodulate the variation in SSSEP carrier signals. The average recognition accuracy was improved by 16.41% using the proposed method compared with the baseline algorithms under the MI-SSSEP paradigm, reaching 81.07%, which far exceeded the 70% BCI application level. Thus, the modulated SSSEP features and proposed algorithms could effectively distinguish the foot motor intention of anatomically adjacent areas and help to expand the application of MI-BCI in the field of lower-extremity motor function rehabilitation.

Abbreviations

brain–computer interface (BCI); Motor imagery (MI); electroencephalogram (EEG); event-related synchronization (ERS); event-related desynchronization (ERD); support vector machine (SVM);k-nearest neighbor (KNN); steady-state somatosensory evoked potential (SSSEP); task-related component analysis (TRCA); filter bank common spatial pattern (FBCSP); interstimulus phase coherence (ISPC); TRCA-based Riemannian geometry method (TRCARIE); TRCA-based SVM method (TRCASVM);FBCSP-based Riemannian geometry method (FBCSPRIE); FBCSP-based SVM classifier (FBCSPSVM); steady-state visual evoked potential (SSVEP)

Declarations

Acknowledgements

The authors would like to thank all the subjects for their participation to this study and for their feedback.

Authors' contributions

YB and HQ designed the experiments. JL and LZ recruited the participants and performed the experiments. YB, HQ and JL analyzed the data. YB, HQ, TG, and XF wrote or edited the manuscript. All authors read and approved the final manuscript.

Funding

This work was supported by the National Natural Science Foundation of China (No. 91648122、82172057) and the Natural Science Foundation of Tianjin (No. 19JCYBJC28700).

Availability of data and materials

The datasets used and/or analyzed during the current study are available from the corresponding author on reasonable request.

Ethics approval and consent to participate

Ethics approval was obtained from the ethics committee of Tianjin University. Consent to participate was obtained from each participant prior to data collection.

Consent for publication

Not applicable.

Competing interests

The authors declare that they have no competing interests.

Author details

[1] Tianjin Information Sensing & Intelligent Control Key Lab, Tianjin University of Technology and Education, Dagu South Road No.1310 ,Hexi District，Tianjin 300222, China; [2] School of Precision Instrument and Opto-electronics Engineering, Tianjin University, Weijin Road No.92, Nankai District , Tianjin 300072, China

References

1. Wolpaw J, Wolpaw E. Brain–Computer Interfaces: Principles and Practice[M]. New York: Oxford University Press, 2012.
2. Cervera M A, Soekadar S R, Ushiba J, et al. Brain-computer Interfaces for Post-Stroke Motor Rehabilitation: a Meta-analysis[J]. Annals of Clinical and Translational Neurology, 2018, 5(5): 651–663.
3. Mihara M, Hattori N, Hatakenaka M, et al. Near-infrared Spectroscopy–mediated Neurofeedback Enhances Efficacy of Motor Imagery–based Training in Poststroke Victims A Pilot Study[J]. Stroke, 2013, 44(4): 1091–1098.
4. Kee Y J, Won D O, Lee S W. Classification of Left and Right Foot Movement Intention Based on Steady-state Somatosensory Evoked Potentials[C].5th International Winter Conference on Brain-Computer Interface (BCI), 2017: 1–3.
5. Rea M, Rana M, Lugato N, et al. Lower Limb Movement Preparation in Chronic Stroke:a Pilot Study Toward an fNIRS-BCI for Gait Rehabilitation[J]. Neurorehabilitation and Neural Repair, 2014, 28(6): 564–575.
6. Jasper H H, Penfield W. Electrocorticograms in Man: Effect of the Voluntary Movement upon the Electrical Activity of the Precentral Gyrus[J]. European Archives of Psychiatry and Clinical Neuroscience, 1949, 183(1): 163–174.
7. Pfurtscheller G, Silva F H. Event-Related EEG/MEG Synchronization and Desynchronization: Basic Principles[J]. Clinical Neurophysiology, 1999, 110(11): 1842–1857.
8. Pfurtscheller G, Brunner C, Schlogl A, et al. Mu Rhythm (de)synchronization and EEG Single-trial Classification of Different Motor Imagery Tasks[J]. NeuroImage, 2006, 31(1): 153–159.
9. Chen Z, Wang Z, Wang K, et al. Recognizing Motor Imagery Between Hand and Forearm in the Same Limb in a Hybrid Brain Computer Interface Paradigm: An Online Study[J]. IEEE Access, 2019: 59631–59639.
10. Gu L, Yu Z, Ma T, et al. EEG-based Classification of Lower Limb Motor Imagery with Brain Network Analysis[J]. Neuroscience, 2020, 436: 93–109.
11. Hashimoto Y, Ushiba J. EEG-based Classification of Imaginary Left and Right Foot Movements Using Beta Rebound[J]. Clinical Neurophysiology, 2013, 124(11): 2153–2160.
12. Tariq M, Trivailo PM, Simic M. Mu-Beta Event-related (de)Synchronization and EEG Classification of Left-right Foot Dorsiflexion Kinaesthetic Motor Imagery for BCI[J]. PLoS One,2020,15(3): e0230184.

13. Liu YH, Lin LF, Chou CW, et al. Analysis of Electroencephalography Event-Related Desynchronisation and Synchronisation Induced by Lower-Limb Stepping Motor Imagery[J]. Journal of Medical and Biological Engineering,2019,39:54–69.
14. Tariq M, Trivailo PM, Simic M. Classification of Left and Right Foot Kinaesthetic Motor Imagery using Common Spatial Pattern[J]. Biomedical Physics & Engineering Express, 2019, 6(1):015008.
15. Müller-Putz G R, Scherer R, Neuper C, er al. Steady-state Somatosensory Evoked Potentials: Suitable Brain Signals for Brain–Computer Interfaces?[J] IEEE Transactions on Neural Systems and Rehabilitation Engineering, 2006, 14:30–37.
16. Yi W, Qiu S, Wang K, et al. Enhancing Performance of a Motor Imagery based Brain-computer Interface by Incorporating Electrical Stimulation-induced SSSEP[J]. Journal of Neural Engineering,2017, 14(2): 026002.
17. Tao X, Yi W, Wang K, et al. Inter-stimulus Phase Coherence in Steady-state Somatosensory Evoked Potentials and Its Application in Improving the Performance of Single-channel MI-BCI[J]. Journal of Neural Engineering,2021, 18:046088.
18. Delorme A, Makeig S. EEGLAB: an Open Source Toolbox for Analysis of Single-trial EEG Dynamics Including Independent Component Analysis[J]. Journal of Neuroscience Methods, 2004, 134(1): 9–21.
19. Duffy F H, Burchfiel J L, Lombroso C T, et al. Brain Electrical Activity Mapping (BEAM): A Method for Extending the Clinical Utility of EEG and Evoked Potential Data[J]. Annals of Neurology, 1979, 5(4): 309–321.
20. Tanaka H, Katura T, Sato H. Task-related Component Analysis for Functional Neuroimaging and Application to Near-infrared Spectroscopy Data[J]. Neuroimage, 2013, 64:308–327.
21. Nakanishi M, Wang Y, Chen X, et al. Enhancing Detection of SSVEPs for a High-Speed Brain Speller Using Task-Related Component Analysis[J]. IEEE Transactions on Biomedical Engineering, 2018,65(1):104–112.
22. Qi H, Xue Y, Xu L, et al. A Speedy Calibration Method Using Riemannian Geometry Measurement and Other-Subject Samples on A P300 Speller[J]. IEEE Transactions on Neural Systems and Rehabilitation Engineering, 2018,26(3): 602–608.
23. Ang K K, Zhang Y C, Zhang H D, et al. Filter Bank Common Spatial Pattern (FBCSP) in Brain-Computer Interface[C]. IEEE International Joint Conference on Neural Networks (IEEE World Congress on Computational Intelligence), 2008: 2390–2397.
24. Yi W, Qiu S, Qi H, et al. EEG Feature Comparison and Classification of Simple and Compound Limb Motor Imagery[J]. Journal of Neuroengineering and Rehabilitation, 2013, 10(1): 106–106.
25. Lee D, Lee H, Park S, et al. Speeding Up SVM Training in Brain-computer Interfaces[C]. International Conference of the IEEE Engineering in Medicine and Biology Society, 2017: 2101–2104.

Figures

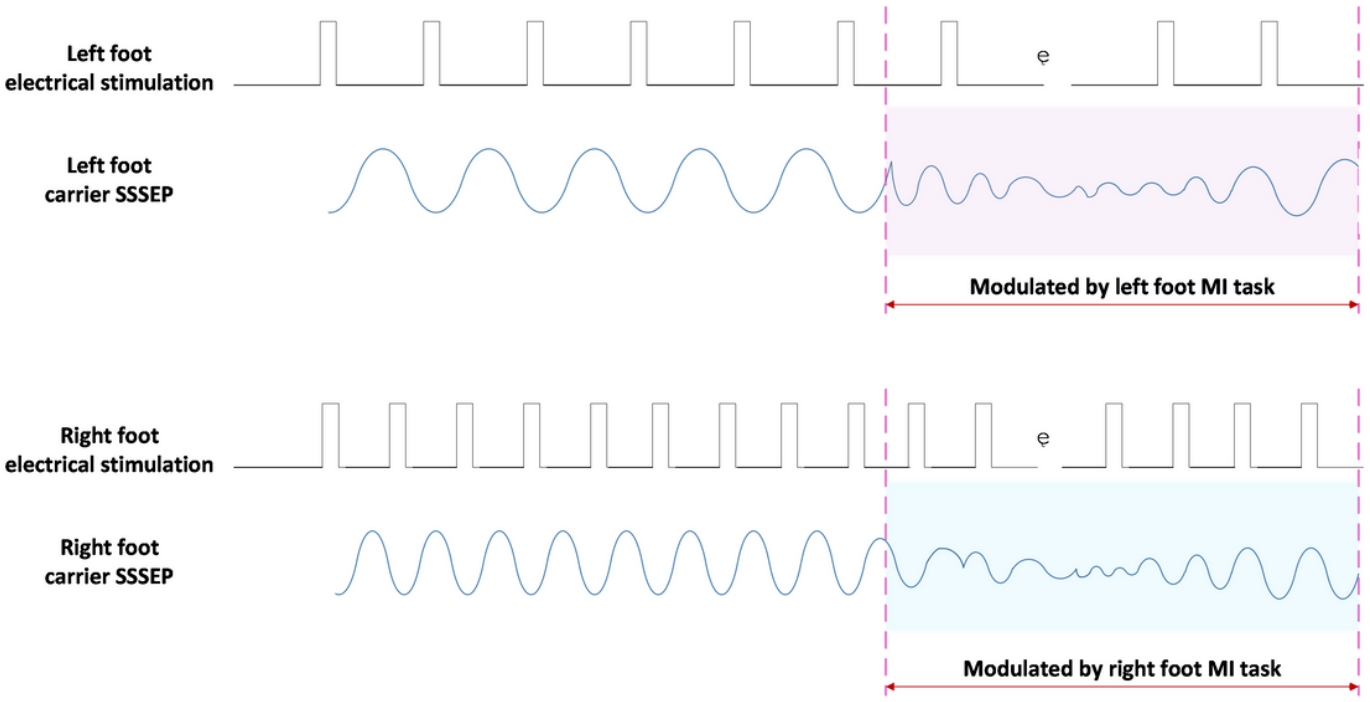

Figure 1

Schematic diagram of lower-limb MI-modulated SSSEPs.

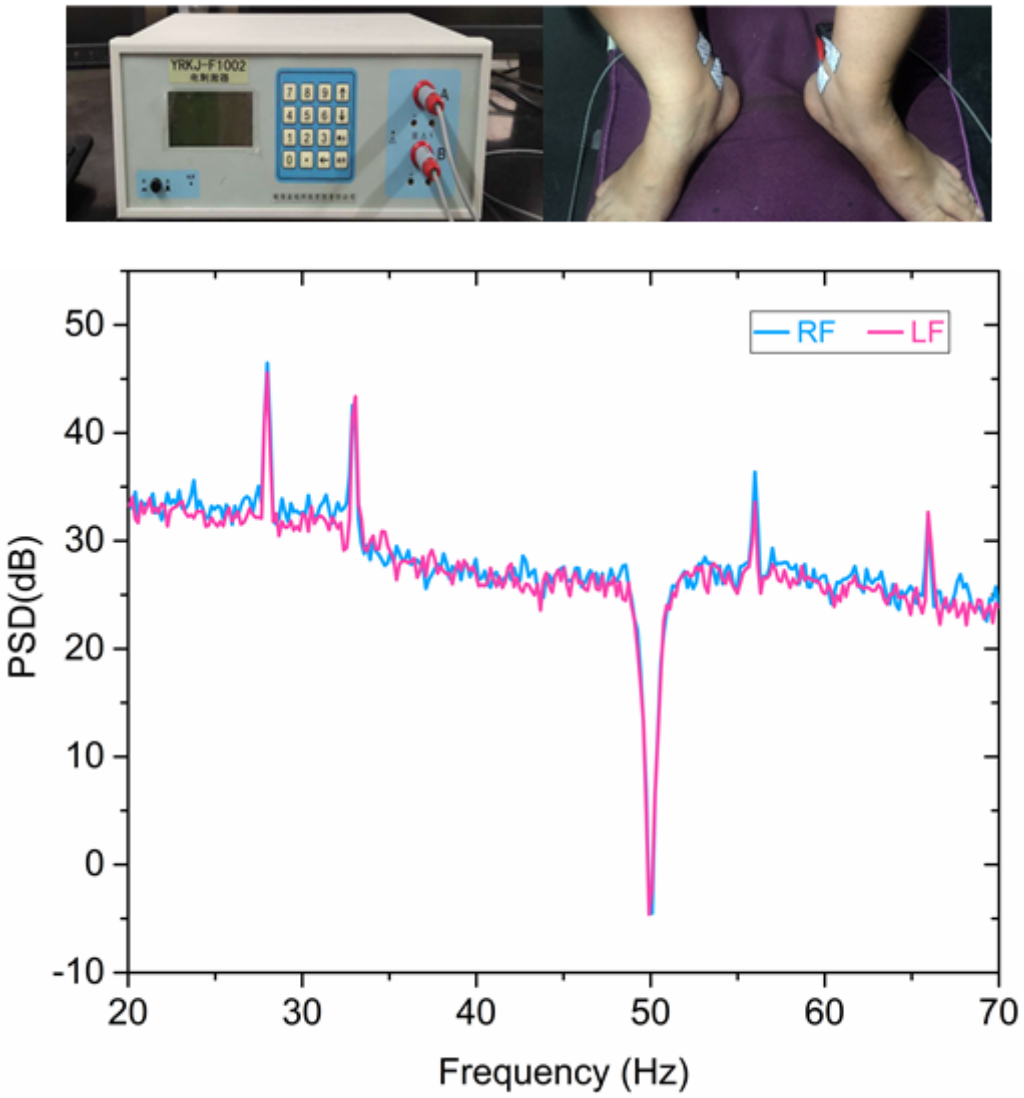

Figure 2

SSSEP evoked by electrical stimulation; ‘RF’ represents the right foot task and ‘LF’ denotes the left foot task.

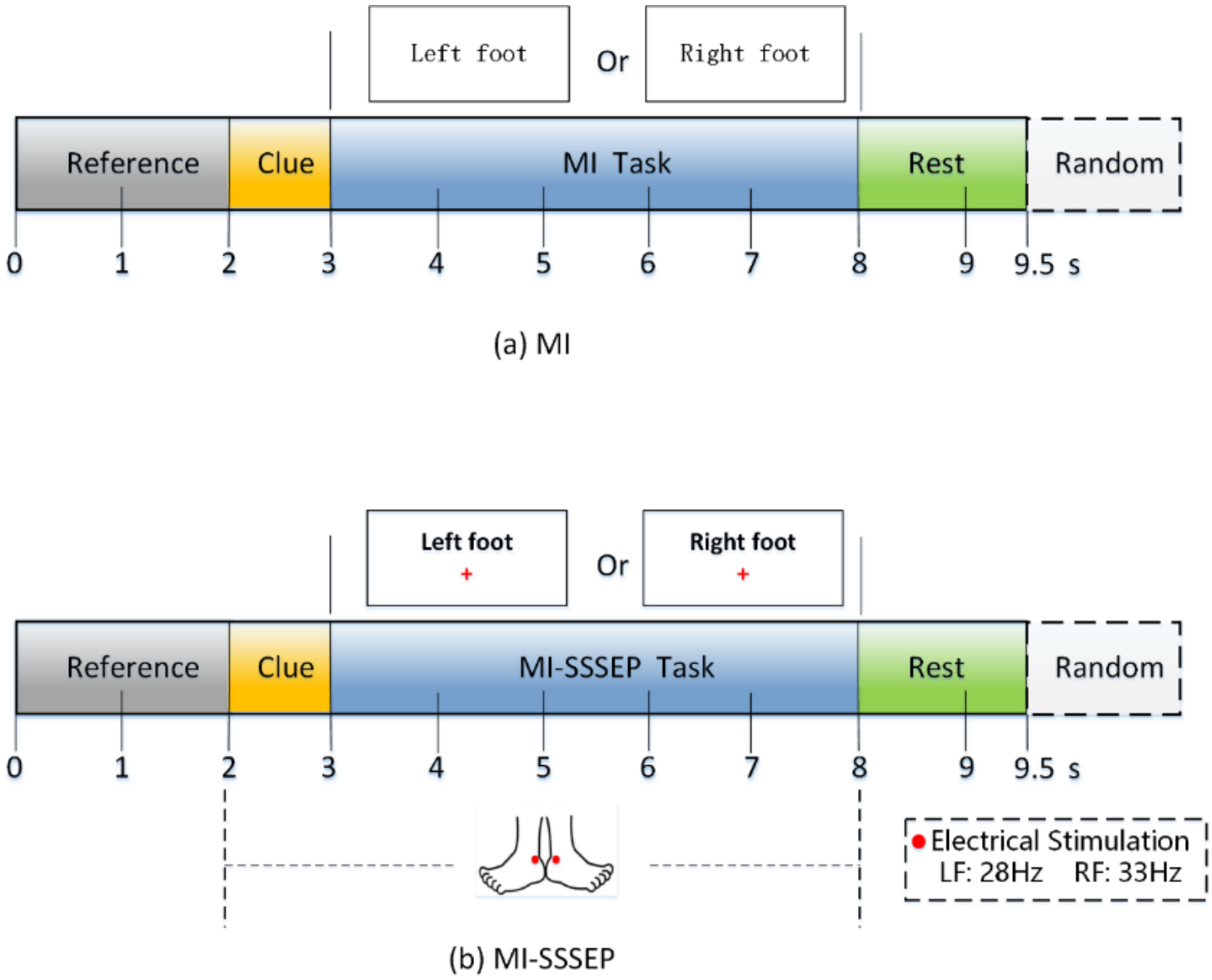

Figure 3

Time course of the experimental paradigms in a single trial.

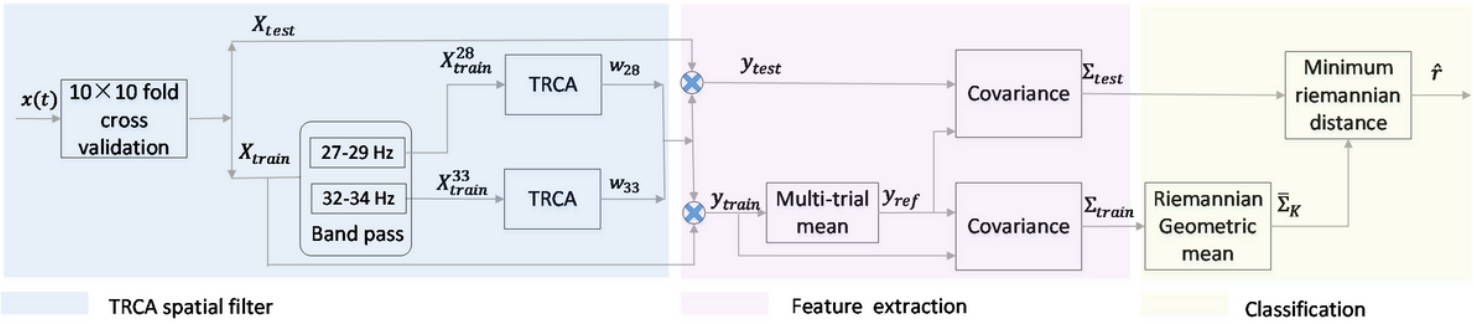

Figure 4

Diagrams of the Riemannian geometry with the TRCA spatial filter method.

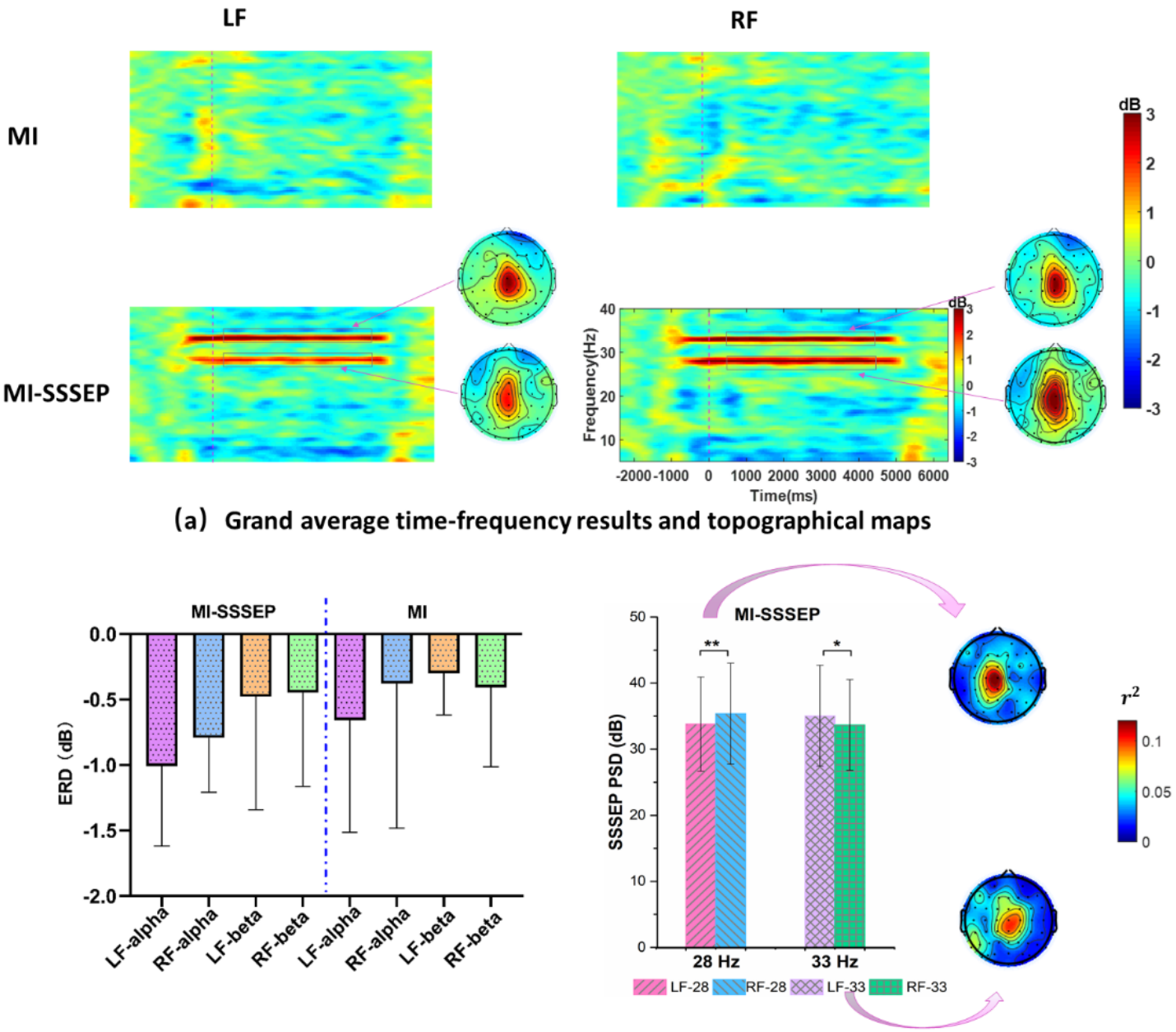

Figure 5

(a) Grand average time-frequency results of the two paradigms on the Cz channel and topographical maps, with the tasks beginning at 0 s; (b) grand average ERD/SSSEP spectrum statistical results between LF and RF on the Cz channel; (c) r^2 coefficient average topographical maps of 28/33 Hz in the MI-SSSEP. “LF” stands for left foot task, “RF” stands for right foot task, “*” means $P < 0.05$, and “**” means $P < 0.01$.

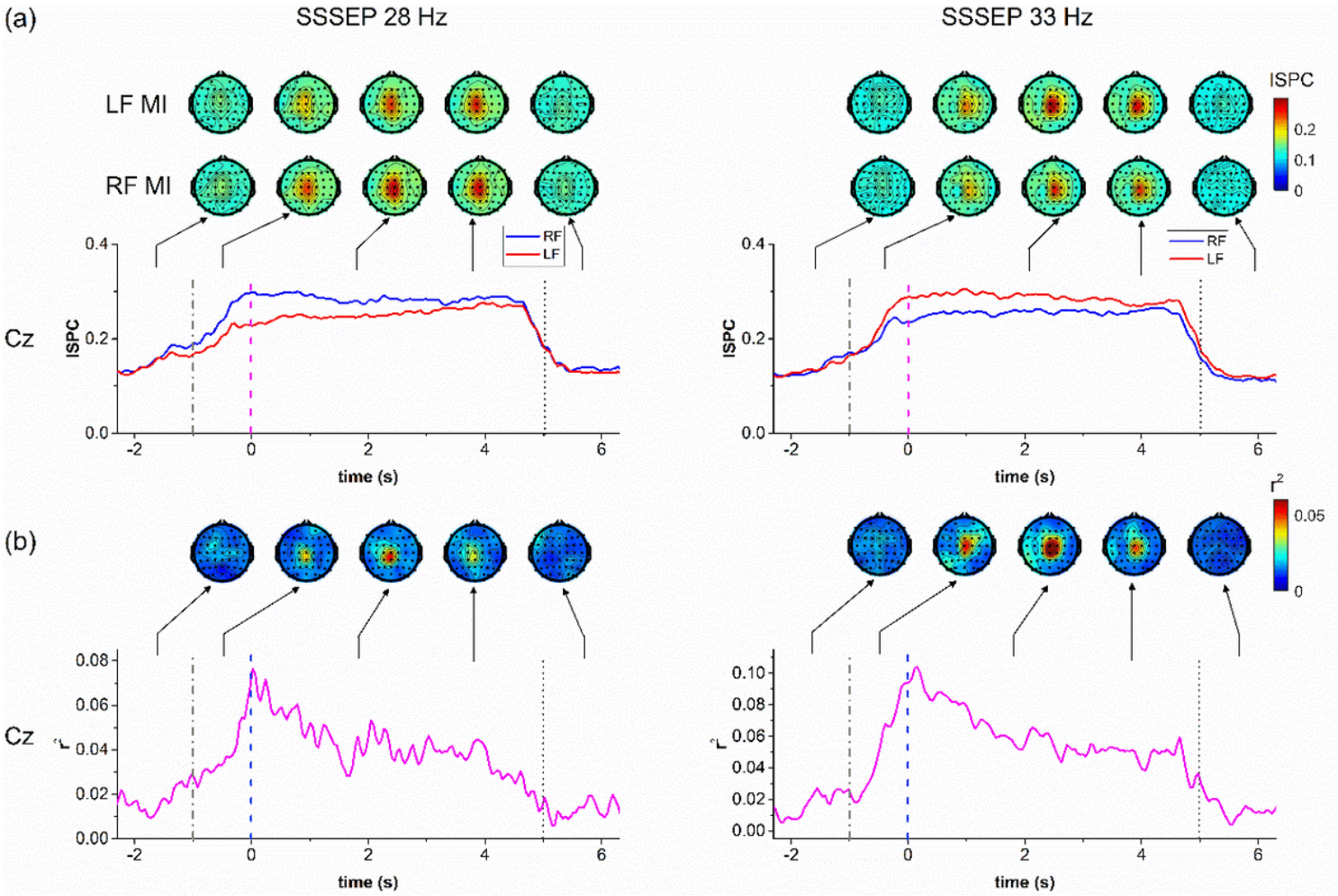

Figure 6

Grand averaged results under the MI-SSSEP paradigm: (a) ISPC curves on the Cz channel and topographical maps at different times between the left and right MI, (b) r^2 coefficient curves between two MI tasks on the Cz channel and r^2 topographical maps at different times. “LF” stands for left-foot imagery task, and “RF” stands for right-foot imagery task. The left panel shows the response at SSSEP 28 Hz, and the right panel shows the response at SSSEP 33 Hz. The three lines in each curve indicate the beginning of electrical stimulation, the beginning of the MI task, and the end of the MI task from left to right. The solid arrows at the top of the curve represent the time corresponding to the topographical maps.

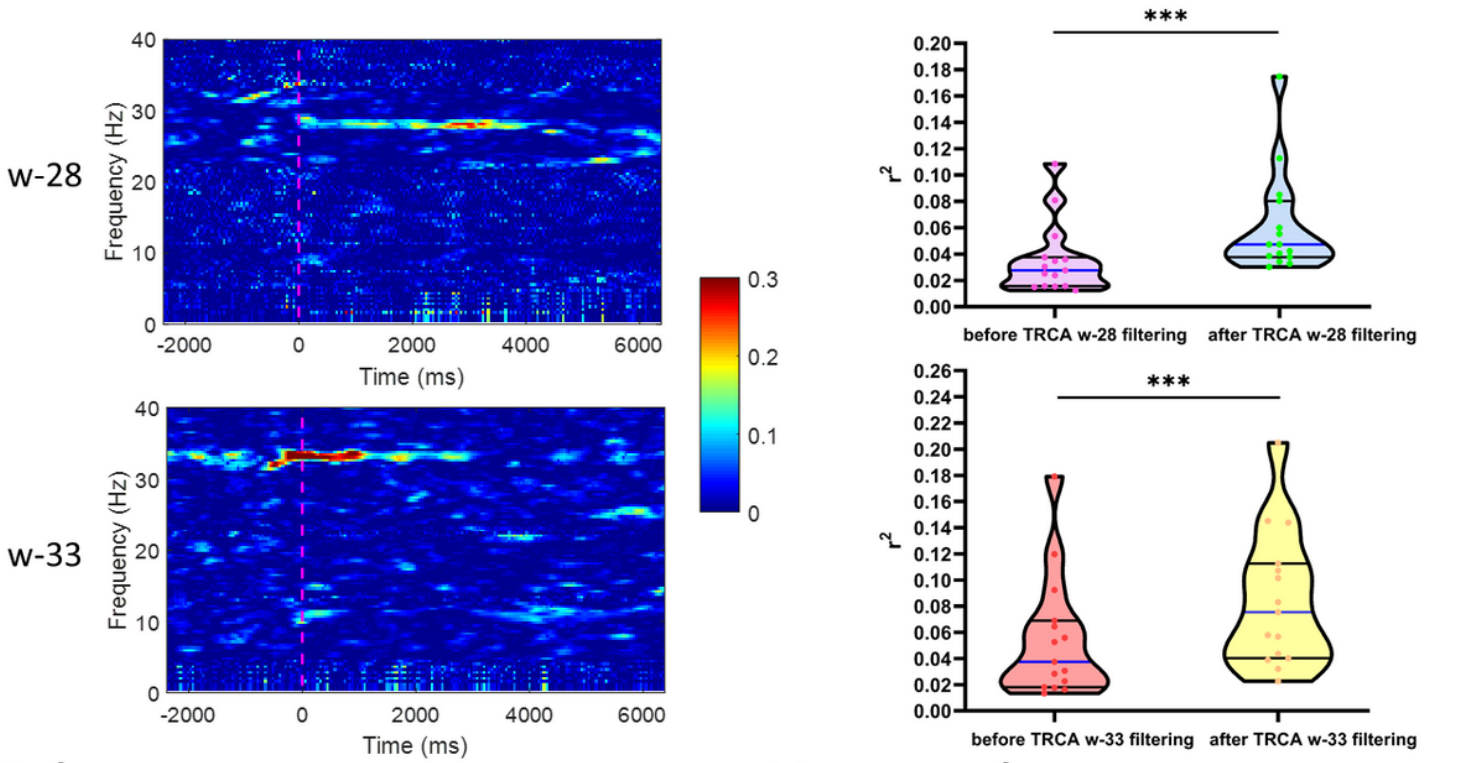

（a） r^2 temporal-frequency map of data filtered by TRCA spatial filter(S4) （b） Grand averaged r^2 comparisons before and after TRCA filtering

Figure 7

TRCA filter analysis, including (a) temporal-frequency maps of data filtered by the SSSEP 28/33 Hz TRCA spatial filter for a typical subject, with “w-28” and “w-33” denoting the TRCA filter at 28 and 33 Hz, respectively, and the purple dotted line representing the beginning of the MI task; and (b) grand average r^2 coefficients before and after the TRCA filter with Wilcoxon signed-rank test. “***” means P < 0.001.

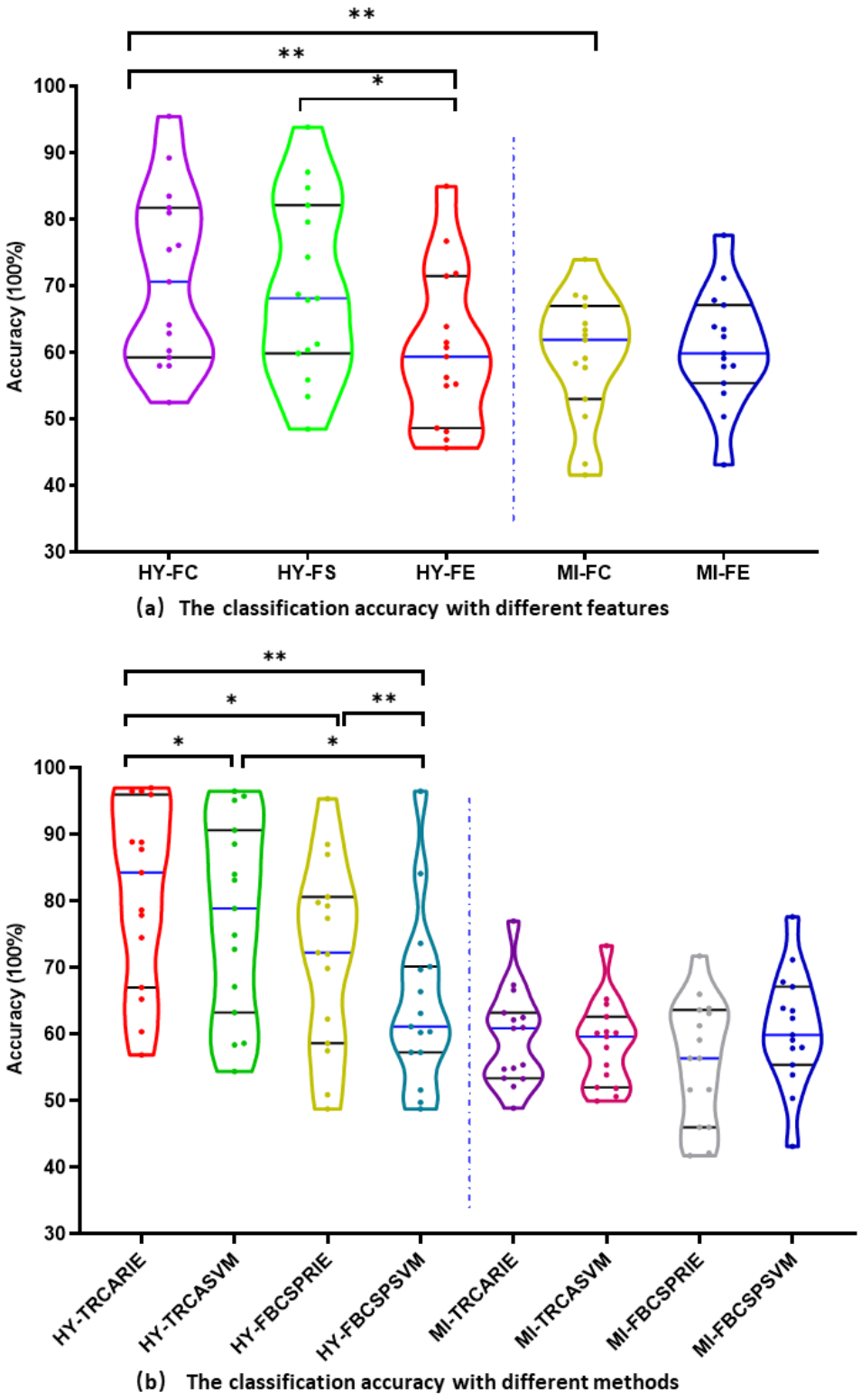

Figure 8

Classification accuracy with (a) different features (using baseline method); “HY” and “MI” represent the results of the MI-SSSEP and MI paradigms, respectively; “FC,” “FS,” and “FE” denote the baseline method classification using both ERD and SSSEP features (six sub-band features), SSSEP features (four sub-band features with first and second harmonic), and ERD features (alpha and beta features), respectively; (b) different methods (using baseband of SSSEP features for MI-SSSEP and ERD features for MI), where

“TRCA/FBCSP” denotes TRCA-based/FBCSP-based feature extraction methods, while “RIE/SVM” represents using a Riemannian/SVM classifier. “**” indicates $P < 0.01$, and “*” indicates $P < 0.05$.